VII International Conference on Computational Methods for Coupled Problems in Science and Engineering
COUPLED PROBLEMS 2017
M. Papadrakakis, E. Oñate and B. Schrefler (Eds)

NUMERICAL SIMULATION OF DROPLET IMPACT EROSION : DANG VAN FATIGUE APPROACH

G. COUDOUEL[1,2,*], A. COMBESCURE[1] AND J.-C. MARONGIU[2]

[1] Laboratoire de Mécanique des Contacts et des Structures (LaMCoS), UMR CNRS 5259
Institut National des Sciences Appliquées de Lyon (INSA)
20 Avenue Albert Einstein, 69100 Villeurbanne, France
e-mail: {guillaume.coudouel - alain.combescure}@insa-lyon.fr, http://lamcos.insa-lyon.fr/

[2]ANDRITZ Hydro
13 Avenue Albert Einstein, 69100 Villeurbanne, France
e-mail: jean-christophe.marongiu@andritz.com, www.andritz.com/hydro.htm

Key words: Impact, Coupling, Droplet, Erosion, Fatigue, FEM, Fluid SPH, Explicit Dynamics

Abstract. The aim of this work is to understand the erosion mechanism caused by repeated water droplets impingement on a metallic structure, and then perform numerical simulations of the damage. When a high velocity water droplet with small diameter impacts a rigid surface, interaction is driven by inertial effects. Upon impact, the "water-hammer" pressure appears by inertial effect at the center of the contact though the maximum pressure occurs on the envelope of the contact area. Lateral jetting occurs by compression when the wave front travelling inside droplet overtakes the contact area. Concerning the structure, erosion is due to fatigue cracking. First, material grains are weakened during an "incubation" phase. After a large number of impacts, micro-cracks emerge and lead to ejection or fracture of grains, what is called "amplification" phase. Numerical simulation including rigid solid allows to locate the most loaded zones of the area, by observing the pressure and mainly the impulse. A 2-way coupling computation with fluid-structure interaction at macroscopic scale allows to confirm the fatigue-based mechanism by observing the hydrostatic stress. Finally, erosion program developed with Dang Van criterion provides the location of the most eroded zones of the structure during a loading cycle. They locate at the edge of jetting zone, which shows the influence of microjets in the erosion mechanism.

1 INTRODUCTION

This work is part of the PREDHYMA project, which concerns the erosion of Pelton turbines buckets. Hydraulic turbines can undergo severe damaging during operation, because of low quality water or detrimental flow conditions. Damaging induces maintenance costs and power production losses, and can also endanger safety of installations. Hydropower plants operators and turbine manufacturers are interested in extending overhaul periods by reducing damaging intensity and protecting turbine components with surface treatments. Accurate and reliable prediction of damaging is however missing. The present work is related to the erosion arising from repeated impacts of high speed water droplets on specific parts of Pelton turbines. Indeed for high head Pelton units, the jet of water is composed of a liquid core surrounded by droplets. Observations show that regions of impact of these droplets exhibit specific erosion patterns. First, the erosion mechanism is described, which allows to highlight the most important phenomena involved in the generation of damage. Then, numerical simulations are performed. They consist of the impact of a water droplet on a metallic structure, with an erosion post-processing.

2 DROPLET IMPACT EROSION

This part explains the mechanism responsible for the wear of metallic structures by water droplets impingement. Firstly, the mechanisms happening into the droplet in case of impact are presented, like the "water-hammer" pressure and waves propagation. The maximum pressure on the wall appears when side jets emerge from the droplet. Then, the erosion mechanism itself inside the solid is presented. These mechanisms may be split into two groups : the damages acting at macroscopic scale, then the mesosopic ones, such as intergranular cracks propagation leading to grain removal or tilting. This last case produces pits on the surface.

2.1 Liquid-solid impact

2.1.1 Waves propagation

According to Haller and Li [5, 10], when a small diameter and high velocity water droplet impacts a rigid flat target, viscous effects and surface tension can be neglected. Indeed, for a droplet radius $R = 0.1$mm and initial velocity $V = 500\text{m.s}^{-1}$, Reynolds number is Re = 50′000 and Weber number is We = 350′000 [5]. Numerical results from Haller [5] show almost constant temperature, so convective heat transfert is not involved in the fluid motion. Therefore, the fluid behaviour is driven by inertial effects and Euler equations can be considered for numerical simulations. After impact, a shock wave starts moving from the contact zone and propagates along the droplet lateral free surface. This wave follows an unobservable triple point, near the contact edge. Field and Haller [3, 5] build the shock front with the geometric principle of Huygens-Fresnel. The front is the envelope of wavelets created by successive edges of the contact (Figures 1.a and 1.b). The volume defined by the wave front and the contact area is highly compressed (Figure 1.a). Concerning the solid body, the droplet impact induces two main types of waves : spherical waves propagate inside volume and Rayleigh waves on the surface. Spher-

ical waves consist into longitudinal compression waves (P-waves), and transverse shear waves (S-waves). S-waves propagate slower than P-waves for most of metals.

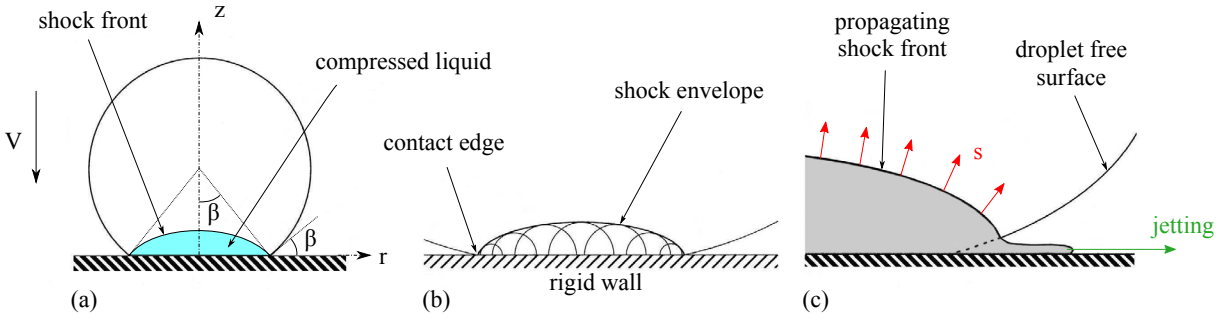

Figure 1: Impact of a spherical droplet on a rigid wall. **(a)** Shock front and highly compressed volume. **(b)** Geometric construction of the waves front. **(c)** Born of lateral micro-jets. (Haller [5]).

2.1.2 Contact pressure and micro-jetting

During the impact of a fluid body on a solid target, the "water-hammer" pressure p_{wh} emerges at the center of the contact area. Field, Heymann, Kennedy and Li [4, 6, 8, 10] give it expression for a rigid solid body in equation (1) :

$$p_{\text{wh}} = \rho_f^0 s V \tag{1}$$

were ρ_f^0 is the initial fluid density, s stands for the compression waves velocity traveling in the droplet (cf. Figure 1.c) and V the normal impact velocity of the droplet. Haller, Heymann and Li [5, 6, 10] approximate s in these conditions and give another expression for p_{wh} with equation (2), where k is a liquid-defendant constant, whose value equals 2 for water, and c_f^0 stands for initial sound velocity in water at room temperature :

$$p_{\text{wh}} = \rho_f^0 c_f^0 V \left(1 + k\frac{V}{c_f^0}\right) \tag{2}$$

Surface tension has no influence on pressure response (cf. 2.1.1) (Haller [5]). Numerical results from Haller [5] and Li [10] show the pressure distribution following the contact area over time. According to Field, Haller, Heymann and Lesser [4, 5, 6, 9], the maximum pressure p_{max} occurs exactly on the edge of the contact area (Figure 2.a). The moment the maximum value acts is not at the start of impingement, but when the shock wave overtakes the contact area. Then, compression with solid leads to jetting by lateral ejection of the fluid (Figures 1.c and 2.b). The maximum pressure locates at the jetting region. These two informations are contained in equation (3) where R_{jet} and t_{jet} are respectively the location and the time of jetting :

$$p_{\text{max}} = p(r = R_{\text{jet}}, t = t_{\text{jet}}) \tag{3}$$

The velocity of the jet can be far higher than the impact velocity V and even the ambient sound velocity c_f^0 (Figure 2.b). Unfortunately analytical expression for maximum pressure does not exist. Numerical results of Haller [5] and Kennedy [8] give respectively $p_{\max} \simeq 2p_{\text{wh}}$ and $p_{\max} \simeq 3p_{\text{wh}}$. However, Haller [5] suggests the time when jets form t_{jet} with the equation (4), where $\hat{s}$ stands for compression waves velocity inside the droplet when jetting :

$$t_{\text{jet}} = \frac{RV}{2\hat{s}^2} \tag{4}$$

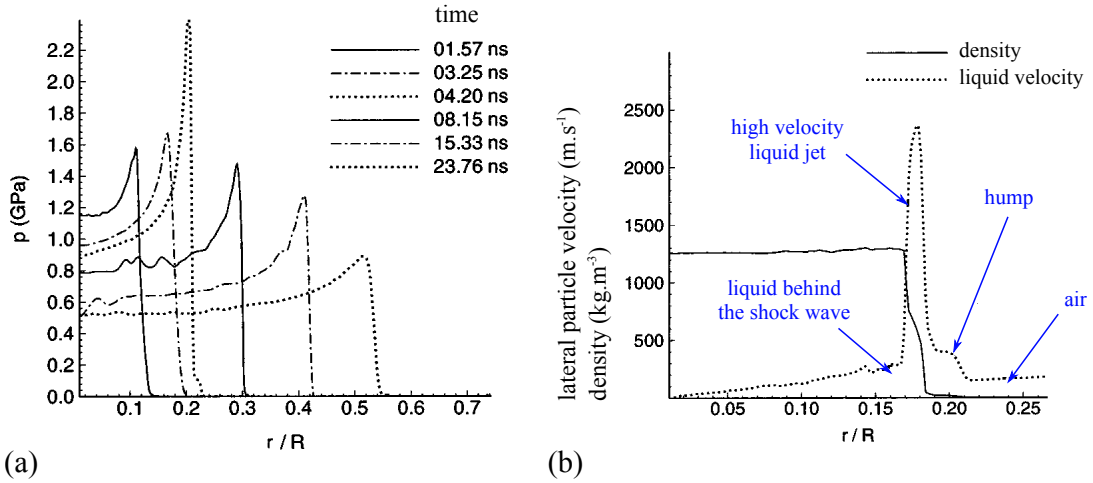

Figure 2: **(a)** Spatial distribution of contact pressure for several times after impact ($R = 0.1$mm, $V = 500$m.s^{-1}). **(b)** Radial velocity and density at the contact zone when jetting. Fluid radial velocity at contact zone (dotted line) shows clearly the jetting initialization at peak location (Haller [5]).

2.2 Erosion mechanism

2.2.1 Macroscopic scale

Claveris [1] worked on droplet impingement erosion of steam turbines blades and splits erosion mechanism into three phases : (i) The first phase is called “incubation period”. During this time no significant loss in mass is observed, but the surface condition changes and becomes more rough. (ii) Then, the loss in mass increases almost linearly until the rate of erosion reach it maximum value and becomes constant. (iii) Finally, erosion rate decreases, possibly again becomes constant, or zero in some cases.

2.2.2 Mesoscopic scale

A mesoscopic description of erosion mechanism is proposed by Kamkar and Luiset [7, 11] as the following steps :

1. The first impacts start to erode grain boundaries and generates pits between grains. Then, microcracks appear at the bottom of these pits.

2. Next, material is removed from surface by two damage modes : a) grain ejection which can produce triple joins, b) grain fracture.

3. After a larger number of impacts, neigbour grains support the same damage mechanism and are ejected or fractured (step 2.). Microckacks are intergranular type, which impair the surface condition, and move in parallel to the surface and propagate in depth. Microvoids born on the surface. The damage zone can be larger than the droplet itself.

4. These defaults are amplified by fatigue.

Finally, erosion is driven by plastic deformation, hardening, intergranular cracks propagation and fatigue mechanism. The cyclic nature of the damage produces a digging by steps (Figure 3).

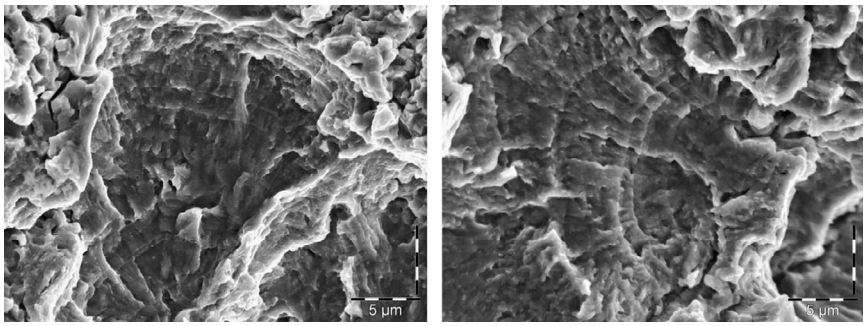

Figure 3: Damage resulting from repeated droplet impacts on stainless steel (Luiset [11]).

3 NUMERICAL SIMULATION OF DROPLET IMPACT EROSION

This section presents the 2D transient simulation of a water droplet impacting on a non-rigid solid body. Then, a fatigue post-processing is performed to estimate the damage over time and therefore the life cycle. The solid dub-domain is computed by the *Finite Elements Method* (FEM) with the explicit dynamics code *EuroPlexus*® [14], which is developed jointly by the french *Commissariat à l'Énergie Atomique et aux Énergies Alternatives* (CEA) and the *European Commission / Joint Research Center* (EC/JRC). This code is suitable for highly non-linear explicit dynamics with erosion. Concerning the fluid sub-domain, *ASPHODEL* code is used. This in-house code developed by *Andritz Hydro* uses the *Smoothed Particle Hydrodynamics* method (SPH) and is efficient to treat free surfaces. The *Fluid-Structure Interaction* (FSI) is performed by the two-way coupling code developed by Nuñez-Ramirez [13], which is energy-conservative at the interface for same time-steps.

3.1 Numerical model features

The solid body consists of a rectangular shaped steel domain. The material considered is homogeneous, isotropic and perfectly bilinear elastoplastic with Young's modulus $E_0 = 200\text{GPa}$, tangent modulus $E_t = 20\text{GPa}$, Poisson's ratio $\nu = 0.228$, yield strength $\sigma_Y = 560\text{MPa}$ and density $\rho_s^0 = 7700\text{kg.m}^{-3}$. The water droplet is a full disc with a radius $R = 0.5\text{mm}$ and moves perpendicularly towards the solid with an impact velocity $V = 100\text{m.s}^{-1}$. The fluid core has a density $\rho_f^0 = 1000\text{kg.m}^{-3}$ and an ambient sound velocity $c_f^0 = 1500\text{m.s}^{-1}$, neither viscosity nor surface tension (see section 2.1.1). Because of the abcense of convective effect (cf. section 2.1.1), the fluid satisfies the Tait equation of state (Macdonald [12]), which is isothermal, where $\gamma_f = 7$ stands for the Grüneisen parameter.

3.2 Droplet impact on a rigid target

Before FSI computation, a fluid computation is performed with the impact of droplet on a rigid wall, in order to understand the nature of loads involved on the solid body. The figure 4.a shows the maximum pressure $p_{\max} \approx 1.7\text{GPa}$, which equals ten times water-hammer pressure calculated with equation (2) and datas from section 3.1, which give $p_{\text{wh}} = 170\text{MPa}$. Maximal pressure locates at $x/R \simeq 0.18$, which corresponds to [5] (see Figure 2). The impulse per unite area, which is calculated by time integration of the pressure, gives a better qualitative idea of load intensity in fast transient dynamics, the load time being responsible for the deformation of surface. The spatial shape of the impulse gives a maximum value at the center of contact and fluctuations are observed at $x/R \simeq 0.18$, because of the instability of signal due to the water ejection. Thus the jetting is located at $R_{\text{jet}} \simeq 0.18 \cdot R = 0.09\text{mm}$.

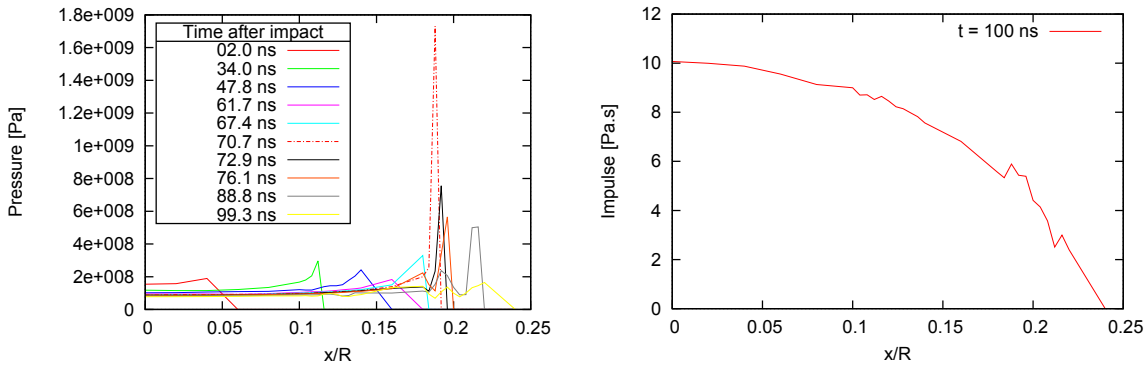

(a) (b)

Figure 4: Load distribution on rigid wall caused by droplet impingement ($R = 0.5\text{mm}$, $V = 100\text{m.s}^{-1}$). Location $x/R = 0$ corresponds to the center of the droplet. **(a)** Pressure distribution on the wall for ten representative times after impact. **(b)** Impulse distribution per unit area on the wall at 100ns after impact.

3.3 FSI computation

3.3.1 Results

Propagation of compression waves is given by observing the evolution and distribution of pressure inside the droplet p_f. A negative pressure corresponds to tension, and positive to compression. Concerning the solid, hydrostatic stress σ_H can be used . Unlike p_f the sign convention of σ_H is the following : $\sigma_H > 0$ in regions subjected to traction and $\sigma_H < 0$ for compression. For solids, shear waves act jointly to compression waves (cf. 2.1.1). They can be observed with the Von Mises stress σ_{VM}. As Von Mises stress stands for the shear intensity and hydrostatic stress gives information about the straction-compression state, these two quantities give general informations about damage by fatigue. Indeed high shear can lead to cracks initiation and a traction state tends to open them (and a compression state to close).

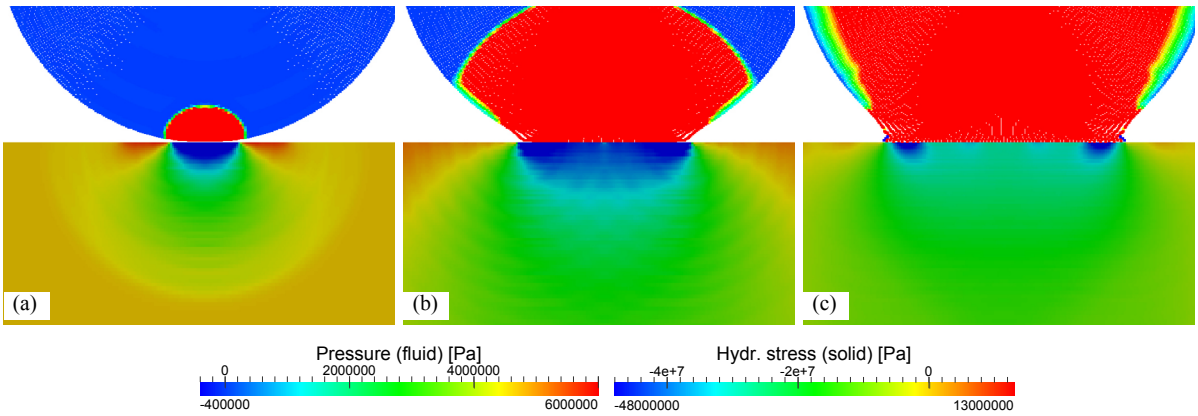

Figure 5: Pressure inside fluid and hydrostatic stress inside solid for several times after impact. **(a)** t = 60ns. **(b)** t = 260ns. **(c)** t = 440ns.

Results show absence of plasticity due to low stress intensity compared to the yield stress (Figures 5 and 6). This assertion is well checked by observing the equivalent plastic strain, which is zero. Analysis of hydrostatic stress allows to globally estimate the type of load inside the solid volume. For a solid region near the surface, the different times of Figure 5 show a change of sign for hydrostatic stress. Indeed, hydrostatic stress in Figure 6.a shows that this region is subject to a traction-compression cycle during the droplet impingement. Figure 6.b shows the shear intensity with the Von Mises stress along time. The value is low compared to yield strength, thus no plasticity occurs in this region.

3.4 Fatigue analysis

3.4.1 Erosion program

The result of simulations allow to define the eroded zones for a given fatigue criteria. After a transient computation, each element of the mesh contains a stress, strains, displacement, etc.

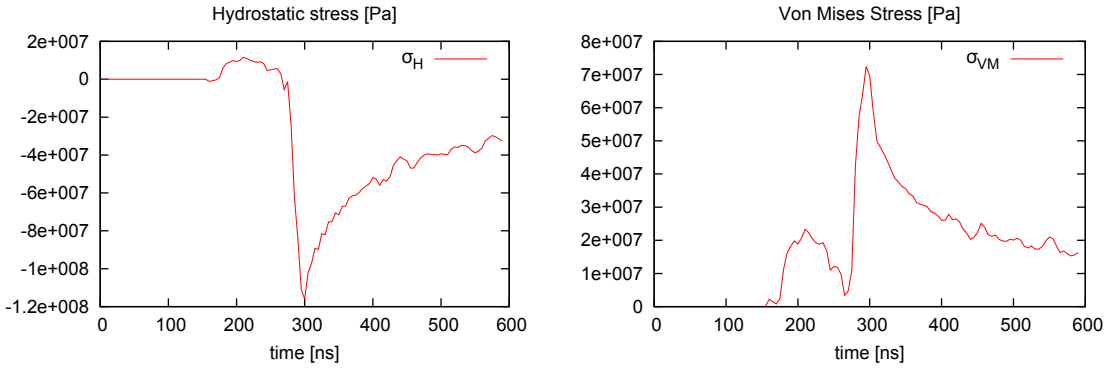

(a) (b)

Figure 6: Stresses at $x = 14.25 * 10^{-5}$m, $z = -2.5 * 10^{-6}$m vs. time. Droplet impacts the solid at $t = 130$ns **(a)** Hydrostatic stress. **(b)** Von Mises stress.

history. These physical quantities are used to define a fatigue criterion, which produces a condition to select which elements of the mesh are eroded and should be removed. This condition is called "fatigue function" and consists into a dimensionless quantity $E \in [0, 1]$. The condition of erosion being $E = 1$, and $E = 0$ corresponding to a virgin element. A fatigue criterion needs a number of load cycles N_{lim} as input, which corresponds to lower limit for non-eroded elements. Fatigue criterion give the opportunity to predict how many identical load cycles N each element can carry before failure. If $N \leq N_{\text{lim}}$, i.e $E = 1$, the element is eroded. This method is a predicting one, and saves a lot of time, because only one load cycle is simulated and not N_{lim}. After removing eroded elements of the mesh, a new FSI interface is computed and another simulation is launched for another number of cycles. The main procedure is detailed on Figure 7. This paper presents only one FSI computation without loop.

3.4.2 Fatigue datas

Generally, resistance to fatigue is checked with a S-N curve such as the Wöhler line (Figure 8), which depends on the material. For a given stress amplitude σ_a, the corresponding number of cycles to failure N is found. If $N \leq N_{\text{lim}}$, fatigue cracking initiates. The fatigue function is then calculated as the ratio between the stress amplitude σ_a and the stress limit σ_{lim}. If E exceeds 1, it value is usually brought back to 1 for more relevance. Indeed, from $E \geq 1$, the element concerned is damaged, regardless of the value of E.

3.4.3 Fatigue criterion

The fatigue damage is evaluated with the second version of Dang Van criterion [2]. The fatigue function E_{DV} is given in equation (5) :

$$E_{\text{DV}} = \sup_t \left\{ \frac{\tau^a(t) + \alpha\sigma_H(t)}{\beta} \right\} \tag{5}$$

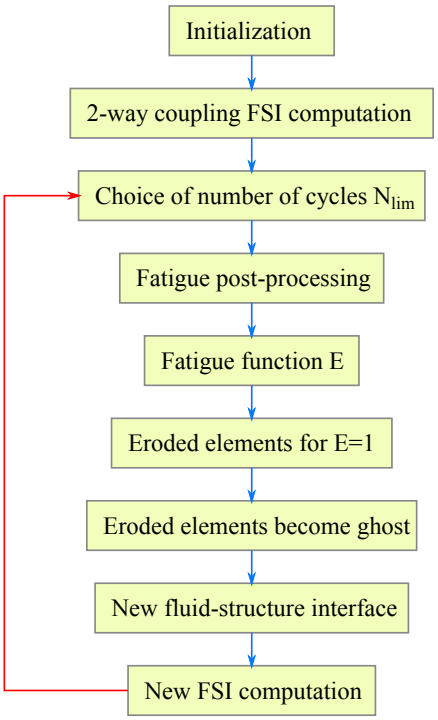

Figure 7: Erosion simulation procedure.

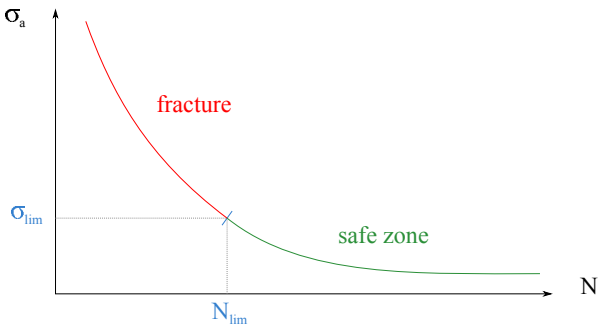

Figure 8: Wöhler line.

Where τ^a stands for shear amplitude and α, β are two coefficients depending on the material given in equation (6) :

$$\alpha = 3\left(\frac{\tau_{-1}}{\sigma_{-1}} - \frac{1}{2}\right) \qquad \beta = \tau_{-1} \tag{6}$$

Where σ_{-1} and τ_{-1} are respectively the endurance limit under symmetrical alternate traction and torsion. As measures for τ_{-1} are difficult to provide, the approximative value $\tau_{-1} = \sigma_{-1}/\sqrt{3}$ is considered. This choice satisfies the validity condition fot the criterion $\tau_{-1}/\sigma_{-1} > 1/2$. It can

be noted that α no longer depends on the material. The shear amplitude τ^a is got by applying the Tresca criterion over the alternate deviatoric stress. Additional informations about shear amplitude are given by Dang [2]. In this study, $\sigma_{-1} = \sigma_{\text{lim}}$. One define commonly the Dang Van equivalent stress σ_{DV} in equation (7) :

$$\sigma_{\text{DV}} = \sup_t \{\tau^a(t) + \alpha\sigma_H(t)\} \tag{7}$$

3.4.4 Results

The results presented in this section concern only one FSI computation and there is no loop described in section 3.4.2. The Dang Van equivalent stress on Figure 9 shows the most loaded zones of the volume, during the load cycle. It maximum value is $\sigma_{\text{DV}} = 30\text{MPa}$. The corresponding number of cycles to failure and damage indicator for $N_{\text{lim}} = 10E6$ are given on Figure 10. It appears that first elements break at 8 millions cycles, i.e. after 8 millions droplets impacts for the following conditions : no change of geometry and the surface is cleaned between each impingement. The eroded zones are enveloping around the jetting area. This results shows the importance of microjets for the erosion mechanism by droplet impact. Thus, the damaged region is crown-shaped. Moreover, erosion acts in depth, because the first elements layer is not eroded. The mesh convergence were checked and there is always a layer of non-eroded elements. But this layer will certainly break after the next impact.

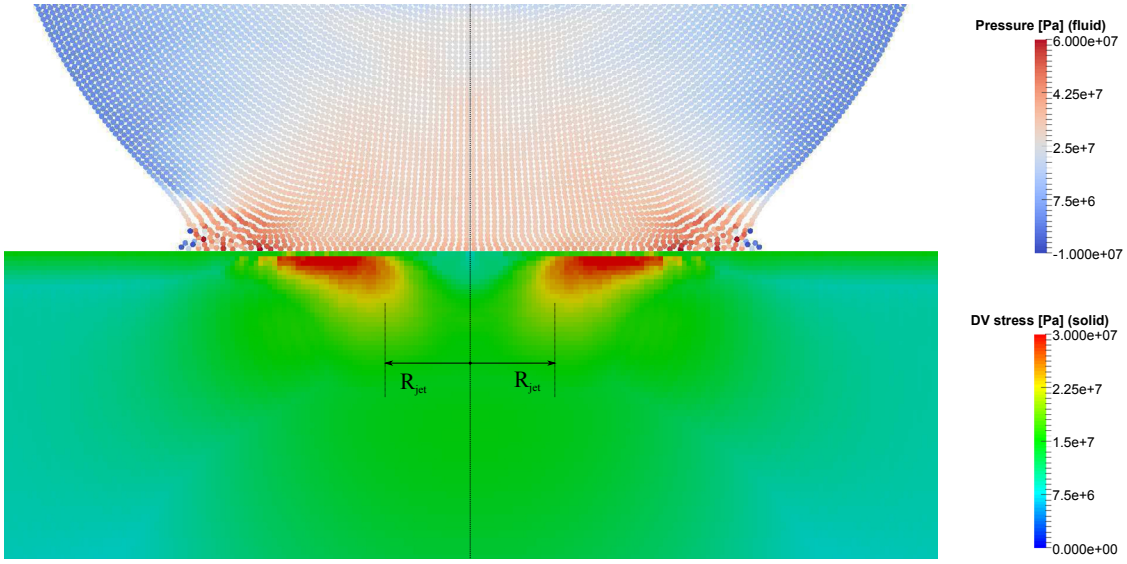

Figure 9: Pressure inside fluid and Dang Van equivalent stress inside solid at $t = 460\text{ns}$ after impact. Mark indicates the position of jetting at $x = R_{\text{jet}}$.

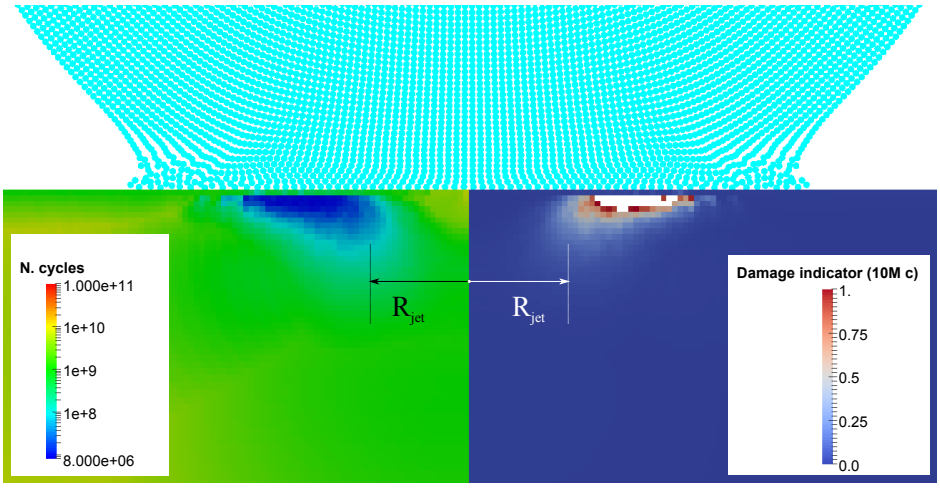

Figure 10: **(Left)** Number of cycles to failure (logarithmic scale) inside solid. **(Right)** damage indicator for $N_{\text{lim}} = 10$M cycles inside solid. Eroded elements are removed from the mesh. Both representations stand for $t = 460$ns after impact. Mark indicates the position of jetting at $x = R_{\text{jet}}$.

4 CONCLUSION

When high velocity droplet with small diameter impacts a rigid target, interaction is driven by inertial effects. Thus, viscous forces and surface tension can be neglected and Euler equations are relevant to represent the fluid behaviour. By inertial effect, water-hammer pressure appears at the center of the contact area, but maximal pressure locates on the contact edge. A compression wave travels inside the droplet, starting from the contact zone. When wave front overtakes contact area, microjets appear near the surface by compression effect. Concerning the structure, erosion is due to fatigue cracking. First, material grains are weakened during an "incubation" phase. After a large number of impacts, micro-cracks emerge and lead to ejection or fracture of grains, what is called "amplification" phase. Numerical simulations are performed subsequently. The droplet impact on a rigid target allows to find the pressure peak and thanks to the impulse, to locate the most loaded zone of the interface. Then, a 2-way coupling FSI computation is build, which gives a general overview of the fatigue mechanism by observing hydrostatic stress. Finally, a fatigue analysis is considered with Dang Van criterion, which supply a forecasting approach by giving informations on structure lifetime. It exposes the erosion shape, which is around jetting zone, showing the influence of microjets on the mechanism of erosion by water impingement. These first results will be a strong basis for a sensitivity analysis on main impact parameters (droplets diameter and velocity). It is also planned to investigate the influence of a thin water layer set on the solid surface to mimic the wet environment, and a multi-layer material to take into account the coated surface of Pelton buckets.

REFERENCES

[1] J. Claverie. *Critère permettant de prévoir le risque dérosion des corps basse pression des turbines à vapeur*, Électricité de France, 1973, ref J/32/062/1.1

[2] Dang Van, K., Griveau, B., Message, O. *On a New Multiaxial Fatigue Limit Criterion: Theory and Application Biaxial and multiaxial fatigue* EGF Publication, 1982, 3, 479-496

[3] J.E. Field. *ELSI Conference: invited lecture: Liquid impact: theory, experiment, applications*, Wear, 1999, 233-235, 1-12

[4] J.E. Field, J.-J. Camus, M. Tinguely, D. Obreschkow, M. Farhat. *Cavitation in impacted drops and jets and the effect on erosion damage thresholds*, Wear, 2012, 290-291, 154-160

[5] K. K. Haller, Y. Ventikos, and D. Poulikakos. *Computational study of high-speed liquid droplet impact*, Journal of applied physics, 2002, 92, 2821-2828

[6] F.J. Heymann. *High-speed impact between a liquid drop and a solid surface*, Journal of Applied Physics, 1969, 40, 5113-5122

[7] N. Kamkar, F. Bridier, P. Jedrzejowski, P. Bocher. *Water droplet impact erosion damage initiation in forged Ti-6Al-4V*, Wear, 2015, 322-323, 192-202

[8] C. F. Kennedy, J. E. Field. *Damage threshold velocities for liquid impact*, Journal of Materials Science 2000, 35, 5331-5339

[9] M.B. Lesser. *Thirty years of liquid impact research: a tutorial review*, Wear, 1995, 186, 28-34

[10] R. Li, H. Ninokata, M. Mori. *A numerical study of impact force caused by liquid droplet impingement onto a rigid wall*, Progress in Nuclear Energy, 2011, 53,7, 881-885

[11] B. Luiset, F. Sanchette, A. Billard, D. Schuster. *Mechanisms of stainless steels erosion by water droplets*, Wear, 2013, 303, 1-2, 459-464

[12] J. R. Macdonald. *Some Simple Isothermal Equations of State*, Rev. Mod. Phys., American Physical Society, 1966, 38, 669-679

[13] J. Nuñez-Ramirez, J.-C. Marongiu, M. Brun, A. Combescure. *A partitioned approach for the coupling of SPH and FE methods for transient nonlinear FSI problems with incompatible timesteps*, International Journal for Numerical Methods in Engineering, 2017, 109, 1391-1417

[14] CEA/DEN/SEMT/DYN *EuroPlexus. A computer program for the finite element simulation of fluid-structure systems under dynamic loading*, Users manual, 2002

Acknowledgement

The research leading to these results has received funding from the European Communitys Seventh Framework Programme (FP7 / 2007-2013) under Grant Agreement 608393 ”PREDHYMA”.